

Self-Powered Sensing for Non-Full Pipe Fluidic Flow Based on Triboelectric Nanogenerators

Siyang He,¹ Zheng Wang,¹ Xiaosong Zhang,¹ Zitang Yuan, Yushan Sun, Tinghai Cheng,* and Zhong Lin Wang*



Cite This: <https://doi.org/10.1021/acsami.1c20509>



Read Online

ACCESS |



Metrics & More



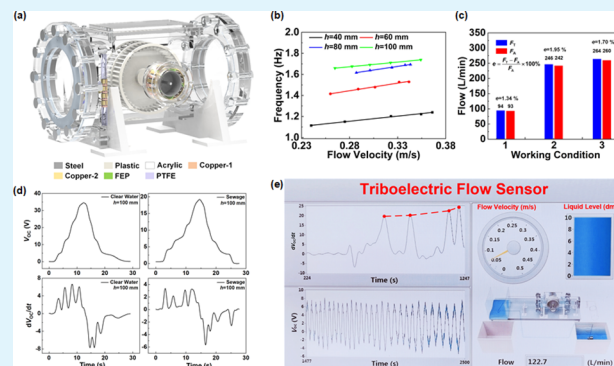
Article Recommendations



Supporting Information

ABSTRACT: Fluidic flow monitoring of a non-full pipe is of great significance in the field of energy measurement and pipeline transportation. In this work, a monitoring method based on triboelectric nanogenerators for non-full pipe fluidic flow of large pipelines is proposed. Specifically, a triboelectric non-full pipe flow sensor (TNPFS) is fabricated, which can monitor the flow velocity and the liquid level simultaneously, and then the flow can be obtained by conversion. For flow velocity monitoring, the flexible blades slide between electrodes, generating periodic electrical signals. Interestingly, the frequencies of the voltage and flow velocities show a good linear relationship. For liquid level monitoring, according to the principle of liquid–solid contact electrification, a variable area interdigital electrode with a stable signal distributed on a polytetrafluoroethylene tube is designed. The experiments demonstrate that the peak number and trend of the voltage derivative curve are related to the liquid level. Finally, a real-time flow-monitoring system is established to effectively monitor the flow from 94 to 264 L/min. Compared with the actual measured flow, the error rate is under 1.95%. In addition to this, the TNPFS also has good responsiveness in sewage. This work provides a novel method for fluidic flow monitoring, especially the non-full pipe flow of large pipelines.

KEYWORDS: triboelectric nanogenerators, fluidic flow monitoring, non-full pipe flow, large pipelines, self-powered sensor



INTRODUCTION

Non-full pipe flow exists in many pipelines, especially in large diameter pipelines, like waste liquid treatment, sewage discharge, and energy transportation.^{1,2} Therefore, it is of great scientific significance to monitor the fluidic flow parameters, such as flow velocity, liquid level, flow, and so on.³ At present, fluidic flow-monitoring technologies mainly include electromagnetic, mechanical, ultrasonic, and so on.⁴ However, these monitoring methods generally have some problems, such as low measurement accuracy of pressure flow sensors, poor anti-interference ability of ultrasonic flow sensors, and high cost of electromagnetic flow sensors.^{5–9} Therefore, it is necessary to propose a novel method for the non-full pipe fluidic flow monitoring of large pipelines.

Wang's group first proposed triboelectric nanogenerators (TEGs) based on the coupling of the triboelectrification effect and electrostatic induction in 2012.^{10–14} The TENGs can effectively obtain energy from nature, such as ocean, vibration, and wind.^{15,16} They can not only collect energy more efficiently in a low-frequency environment^{17–19} but also have the advantages of no external energy supply and low cost.²⁰ In addition, TENGs can also be used as a self-powered sensor.^{21–26} They have been widely applied, such as driving

state sensing,^{27–29} liquid level sensing,^{30–33} flow sensing,^{33–37} chemical sensing,^{38,39} flow rate sensing,^{40–45} pressure sensing,^{46–48} and so on.^{49–52} Among them, flow sensors have been widely developed. For example, Wang's group designed a water-fluid-driven rotating TENG (WR-TENG) for pipeline flow monitoring. In addition, it can also be used for rust removal and scale prevention.⁵³ Chen's group designed a triboelectric microfluidic sensor (TMS), which can monitor not only gas flow but also liquid flow.⁵⁴ However, to date, the monitoring of large pipeline fluidic flow based on TENGs, especially non-full pipe flow, has not been reported.

In this work, a monitoring method based on TENGs for non-full pipe fluidic flow of large pipelines is proposed, and a triboelectric non-full pipe flow sensor (TNPFS) is fabricated, which can monitor the flow velocity, liquid level, and flow simultaneously. The TNPFS consists of an acrylic cylinder, a

Received: October 24, 2021

Accepted: December 28, 2021

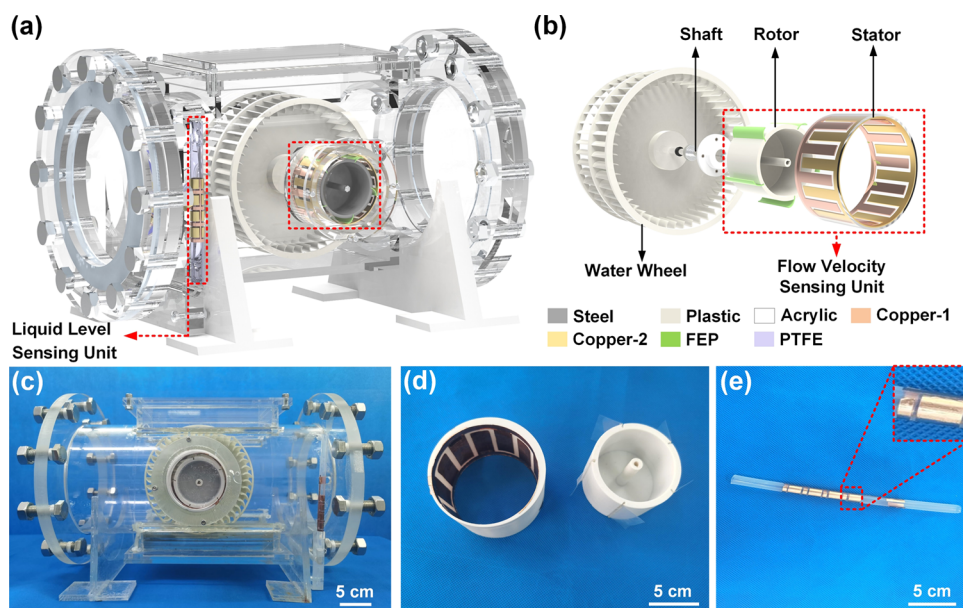


Figure 1. Structure design of the TNPFS: (a) schematic diagram of the TNPFS fabricated for flow monitoring; (b) detailed schematic diagram of the water wheel structure with the TNPFS; and (c–e) physical photos of the TNPFS and the sensing units.

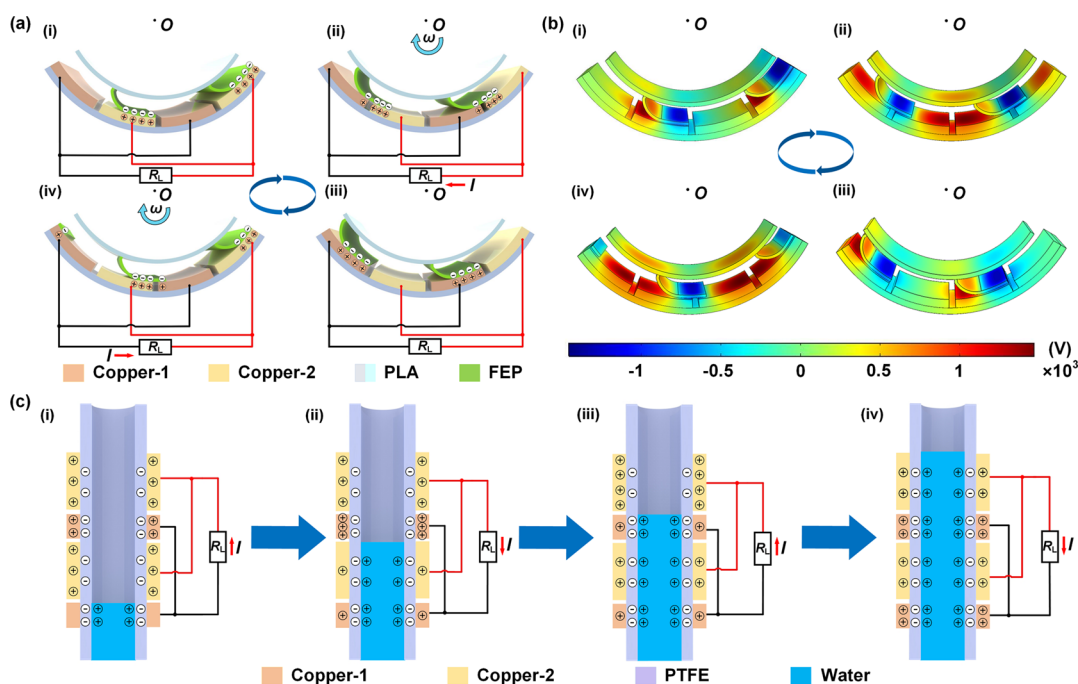


Figure 2. Flow-monitoring principle of the TNPFS: (a) working principle of the flow velocity-sensing unit; (b) simulation results of COMSOL potential distribution of blades at different electrode positions; and (c) working principle of liquid level monitoring.

water wheel structure, and sensing units. First, the relationship between flow velocity and electrical output at several specific liquid levels are investigated. According to the good linear relationship between characteristic frequency and different flow velocities, the frequency can be used as an index to monitor flow velocity. Second, the influence of several different electrode distributions on the stability of liquid level monitoring are experimentally investigated. Comparing with other electrode distributions, a variable area interdigital electrode with good stability is selected to monitor the liquid level. Finally, a flow-monitoring system with real-time interface display of fluidic flow parameters is established, which can

effectively monitor the flow from 94 to 264 L/min. In addition to this, it is verified that the TNPFS also has good responsiveness in sewage. Therefore, this work promotes the development of TENGs in the field of fluidic flow monitoring in large pipelines.

RESULTS AND DISCUSSION

Structure Design and Working Principle of the TNPFS. The overall structure of the TNPFS (Figure 1a) consists of a water wheel rotating structure, a transparent acrylic cylinder, a liquid level-sensing unit, and a flow velocity-sensing unit. The flow velocity-sensing unit adopts the flexible

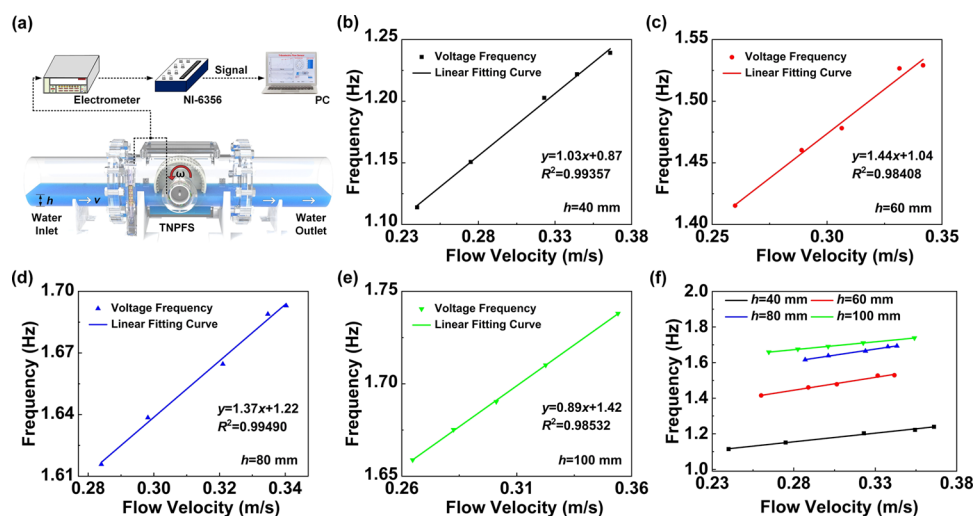


Figure 3. Performance of the TNPFs for flow velocity monitoring: (a) schematic diagram of the non-full pipe flow-monitoring system; (b–e) frequency variation at different flow velocities when the liquid level is $h = 40\text{--}100$ mm; and (f) relationship between velocities and frequencies at different liquid levels.

contact paddle structure to reduce the wear,^{55,56} and the liquid level-sensing unit adopts the way of liquid–solid contact electrification, which can effectively reduce the wear.^{32,46,57} The structural design of the sensing units has good durability and maintainability. The liquid level-sensing unit is connected to the flow channel of the acrylic cylinder through an L-type acrylic connector (Figure S1, Supporting Information). The liquid level in a polytetrafluoroethylene (PTFE) tube is consistent with that in the acrylic cylinder and flows through the electrode parts of the liquid level-sensing unit during flow increase/decrease, and the water wheel structure is axially positioned through the bearing seat and fixed on the sidewall of the acrylic cylinder. Figure 1b indicates the details of the water wheel structure. One side of the shaft is connected with the rotor of the flow velocity-sensing unit, and the water wheel under the driving of water drives the rotor to slide between the copper electrodes of the stator. Figure 1c–e illustrates photographs of the TNPFs, including its overall structure and sensing units.

Figure 2 illustrates the triboelectric conversion mechanism of the TNPFs. To better explain the working principle of the flow velocity-sensing unit, it is described step by step as shown in Figure 2a. In the initial state, when the flexible blades overlap with copper-2 [Figure 2a (i)], they receive negative induced charges by triboelectrification, and the copper electrodes become positively charged. Then, when the flexible blades slide toward copper-1, the electrostatic balance is broken and a potential difference occurs between the electrodes [Figure 2a (ii)]. The flexible blades continue to slide until they overlap with copper-1 [Figure 2a (iii)]. Due to the change in potential difference, negative charges are transferred between electrodes to achieve an electrostatic balance. Finally, when the rotor continues to rotate, the negative charges on copper-1 are transferred to copper-2 through an external circuit [Figure 2a (iv)]. The above is the complete cycle of the power generation of the flow velocity-sensing unit. To verify the principle of the flow velocity-sensing unit, the finite element simulation of fluorinated ethylene propylene (FEP) blades at different positions is carried out (Figure 2b). The potential distribution is consistent with the principle analysis.

Figure 2c introduces the basic working principle of the liquid level-sensing unit. The liquid level-sensing unit is composed of a PTFE tube and a variable area interdigital electrode. Before water enters the PTFE tube, since PTFE easily gain electrons compared to copper, the copper electrodes will generate negative and positive charges with the same density, respectively. In this state, it is in an electrostatic balance. First, when water flows into the PTFE tube, it breaks the electrostatic balance and makes the water near the tube positively charged. Due to the potential difference, electrons are transferred from the small electrode to the large electrodes [Figure 2c (i)]. Second, with the increase of the liquid level, when water flows through the large electrode part of the interdigital electrode, the potential difference will drive electrons from the large electrode to the small electrodes [Figure 2c (ii)]. When the liquid level continues to rise, as shown in Figure 2c (iii, iv), the electron transfer will repeat the previous process. Similarly, when the liquid level decreases, the electrons flow direction is opposite to that when the liquid level increases. To better describe the working mechanism of liquid level monitoring, the potential distribution on the PTFE tube under different liquid levels is simulated by COMSOL Multiphysics software, which is illustrated in Figure S3.

Performance of the TNPFs. To describe the characteristics of the flow velocity-sensing unit, its electrical output at different liquid levels in the experimental system is investigated. As shown in Figure 3a, the experimental system connects the TNPFs with the inlet and outlet water pipes through flanges. The water pump is located at the water outlet to supply water to the water inlet. The flow velocity is adjusted by the water pump, and the liquid level is controlled by adjusting the height of the replaceable plugboard, and the collected electrical signals are transmitted to the PC for display. Figure 3b–e shows the relationship curve between open-circuit voltage frequency and different flow velocities in the range of the liquid level 40–100 mm with per step increasing by 20 mm, and the open-circuit voltage, short-circuit current, and transferred charges in this range are also measured (Figure S4). For the measured voltage, the corresponding characteristic frequency can be calculated by fast Fourier transform (FFT).⁵⁸ Due to the limitation of pump power, the

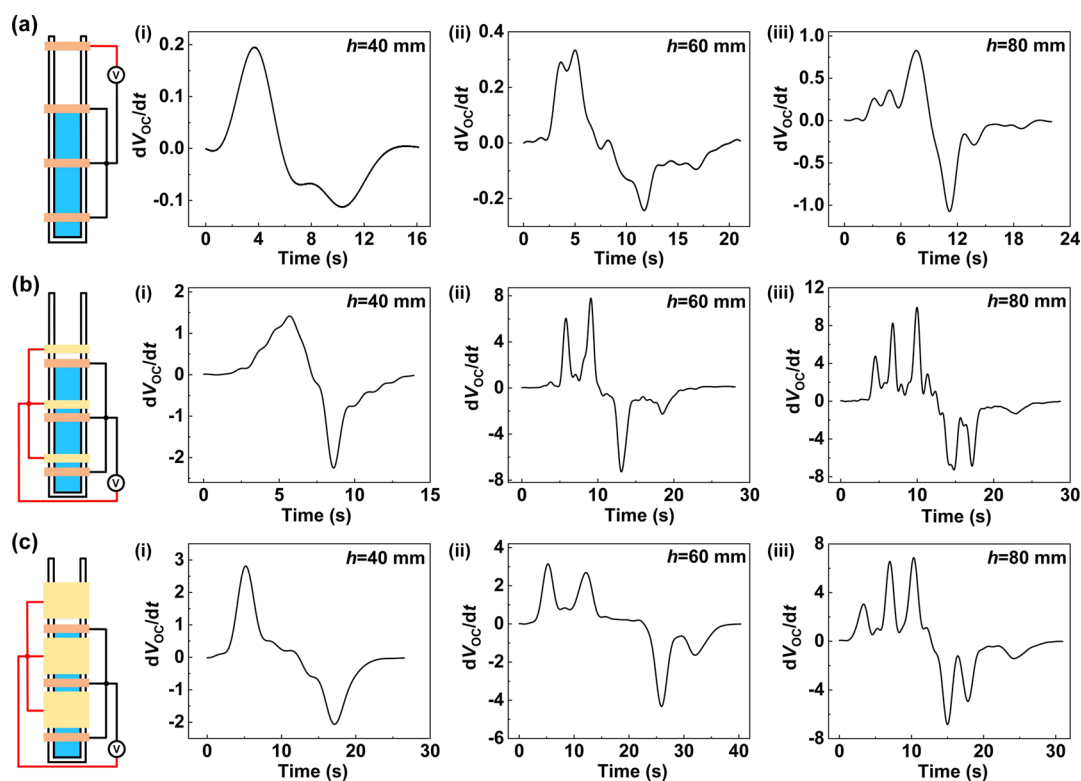


Figure 4. Derivative of open-circuit voltage to time (dV_{OC}/dt) curves of three liquid level-monitoring methods under different liquid levels: (a) electrodes proposed by Zhang et al;³² (b) ordinary interdigital electrodes; and (c) variable area interdigital electrodes at different liquid levels, respectively.

measurement range of flow velocity is limited, but the linearity of characteristic frequency and flow velocity has a good relationship. Therefore, it is shown that the TNPFs can express the flow velocity by the frequency of the voltage. Figure 3f illustrates a summary of flow velocities and characteristic frequencies at different liquid levels. Interestingly, the frequency increases with the increase of the liquid level at the same flow velocity. This is mainly because the higher the liquid level, the more the wheel teeth are impacted by water. Therefore, the greater the force on the water wheel, which causes the increase in the rotation speed of the water wheel. The theoretical derivation of the force on the water wheel is given in eq S10–S17 of the Supporting Information.

To investigate the performance of TNPFs liquid level monitoring, the electrical outputs of electrodes with different distributions at several specific liquid levels are measured, respectively, as shown in Figure 4, and their specific parameters are introduced in the Experimental Section. The variation of the liquid level in the tube is regulated by the water pump. Due to the different open-circuit voltage slopes that result when water flows through different electrode areas or electrode gaps, when the liquid level is increased or decreased, the curve of the derivative of the voltage to time (dV_{OC}/dt) generates positive peaks or negative valleys, which correspond to the distribution of the electrodes significantly. Therefore, the dV_{OC}/dt signals can be used to identify the liquid level. As shown in Figure 4a–c and Figure S6, it is obvious that the liquid level-monitoring method using interdigital electrodes with a variable area has high stability and great advantages as an index to identify the liquid level, and the open-circuit voltage corresponding to the different distributions of electrode modes at different liquid levels is shown in Figure S5.

To further investigate the influence of the variable area interdigital electrodes on the output performance of liquid level monitoring, the dV_{OC}/dt signals of interdigital copper electrodes with area ratios of 1:3, 1:1, and 3:1 at different liquid levels are measured experimentally, as shown in Figure 5. The experimental results demonstrate that the larger the area ratio of interdigital electrodes, the more obvious the relationship between the pulse numbers of the dV_{OC}/dt curve and the

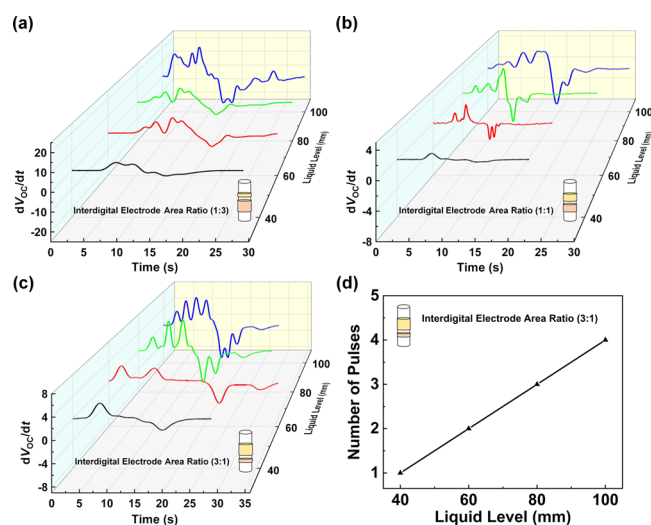


Figure 5. Electrical signals of dV_{OC}/dt at different liquid levels: (a–c) interdigital electrodes with different area ratios and (d) relationship between the liquid level of the variable area interdigital electrodes and electric pulse numbers.

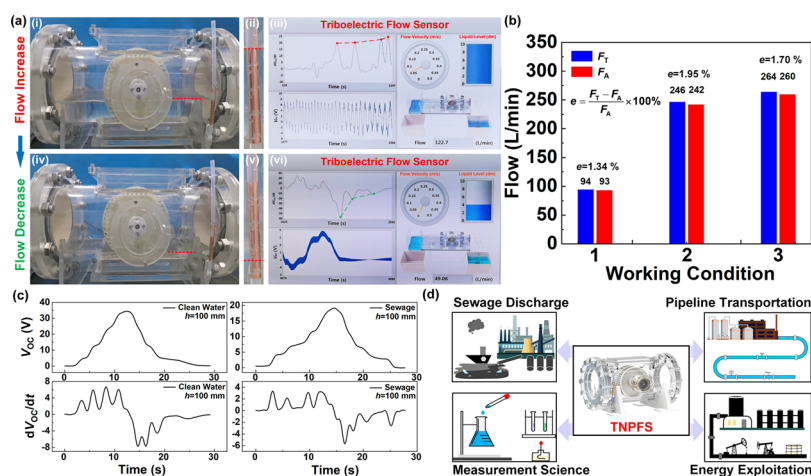


Figure 6. Application of the TNPFs: (a) display of actual flow and the program interface of the flow-monitoring system; (b) comparison between the triboelectric flow sensor and the actual measured flow; (c) performance comparison of liquid level monitoring in clean water and sewage; and (d) application prospect of the TNPFs in the future.

electrodes (Figure 5a–c). When the area ratio of interdigital electrodes is 3:1, the number of pulses is positively correlated with the change of the liquid level (Figure 5d). This is mainly because the fluctuation of water in the large electrodes has little effect on the electrical signal, and the larger the difference of the areas, the larger the electron transfer difference, so it will make the peak more obvious. However, if the interdigital electrode area ratio is too large, the measurement accuracy will be disturbed.

Therefore, to improve the stability of TNPFs liquid level monitoring, the influence of the blank areas of the PTFE tube on the electrical output of liquid level monitoring is investigated. Three kinds of interdigital electrodes with different blank areas are designed. Figure S7 illustrates dV_{OC}/dt signals with copper electrode widths of 3, 5, and 7 mm at different liquid levels, respectively. It is found that the larger the area of copper electrodes covered with a PTFE tube between a pair of electrodes, the smaller the influence of water fluctuation interference on the signal. Therefore, using variable area interdigital electrodes to monitor the liquid level has good stability.

DEMONSTRATION

Figure 6 demonstrates the applications of the TNPFs in flow monitoring. To monitor the flow of the TNPFs under random flow, the function of flow monitoring is realized by programming in LabVIEW software. The program interface and flowchart are shown in Figure 6a and Figure S8 (Supporting Information), which displays the relevant information of instantaneous flow and introduces the operation process of the program. Additionally, a demonstration video of flow monitoring is provided in Supporting Video S1 (Supporting Information). The open-circuit voltage of the flow velocity-sensing unit is measured in real-time by the flow velocity-monitoring program, and the frequency of the open-circuit voltage is calculated by FFT. The correlation coefficient k_i between different flow velocities and frequencies is identified according to the net pulse number N , and the flow velocity is calculated. Meanwhile, the liquid level-monitoring program differentiates the voltage signal of the collected liquid level-sensing unit and outputs the filtered dV_{OC}/dt signal. When the flow increases, the water flows through the electrode

part. Due to the change in the open-circuit voltage, the dV_{OC}/dt signal curve will produce a positive pulse. When the flow decreases, a negative pulse will be generated. The program identifies the liquid level by analyzing the number of positive and negative pulses, and the flow q_V can be determined as follows:

$$q_V = \left(\frac{D}{2}\right)^2 \times \left[\arccos\left(\frac{D - 2aN}{D}\right) - \frac{1}{2} \sin\left(2\arccos\left(\frac{D - 2aN}{D}\right)\right) \right] \times k_f f_i \quad (1)$$

where a is the coefficient between the N and h , D is the diameter of the TNPFs, and f_i is the frequency of the open-circuit voltage calculated by FFT. The detailed derivation of the flow formula is given in eqs S1–S8 of the Supporting Information, and under three different flows, the detailed comparison between the flow F_T measured by the TNPFs and the actual measured flow F_A (Figure 6b) shows that the flow value obtained from the TNPFs is very consistent with the actual measured flow value, and the error rate ϵ is under 1.95%. The actual measured flow F_A is obtained by measuring the volume of water flowing from the outlet to the water tank within a certain time.

Moreover, as a large pipeline flow sensor, the TNPFs should also have a good response in sewage. The flow velocity-sensing unit and the liquid are two independent spaces and they will not interfere with each other. Therefore, the performance of liquid level monitoring in sewage is investigated systematically. The voltage output characteristics and dV_{OC}/dt signals of the TNPFs liquid level-sensing unit in clean water and sewage are measured, respectively. As shown in Figure 6c, the voltage pulse signal still corresponds to the liquid level. Therefore, the performance of flow monitoring will not be affected by sewage, and the TNPFs can be used as a stable flow-monitoring method. Meanwhile, the durability of the TNPFs is tested. It is proved that the output voltage peak remains almost unchanged after working for 4 h (Figure S9, Supporting Information). However, the TNPFs also faces some challenges, such as in the environment with a large amount of sediment. It has broad development and application prospects in the fields of energy exploitation, sewage discharge, pipeline transportation, and

measurement science (Figure 6d). For example, in measurement science, since the performance of the sensor is not affected by the medium, it has the potential to transport strong acid and strong alkali solutions in future research; in the field of sewage measurement, it has the potential to detect sewage concentration; in the field of energy exploitation, the state of liquid energy can be monitored and even the flow of some solid particles; and in the field of pipeline transportation, the flow switch can be remotely controlled according to the flow to realize the reasonable distribution of flow. This work provides a new alternative means for intelligent flow monitoring.

CONCLUSIONS

In summary, a monitoring method for fluidic flow of non-full pipes is proposed and analyzed. Based on this, a triboelectric flow sensor is manufactured to monitor the fluidic flow in large pipelines. When the flow changes, the sensing unit of the TNPFs generates corresponding electrical signals, respectively. For the flow velocity-sensing unit, the voltage frequency has a good linear relationship with the flow velocity, which proves the feasibility of flow velocity monitoring. The liquid level-sensing unit of the TNPFs uses liquid–solid contact electrification, and a variable area interdigital electrode is designed, which has good stability compared with other methods of electrode distribution. Finally, from the demonstration experiment, the real-time flow monitoring is established, which can effectively monitor the flow from 94 to 264 L/min. In addition, the sensor also has a good response in sewage. This work provides a novel alternative means for fluidic flow monitoring and further promotes the development and application of TENGs in the field of fluid engineering.

EXPERIMENTAL SECTION

Fabrication of the TNPFs. The outer cylinder (inner diameter 200 mm, outer diameter 220 mm, thickness 10 mm, and length 90 mm) is made of acrylic material. The water wheel (220 mm diameter and width 105 mm) is connected to the bearing block fixed on the outer cylinder by a stainless-steel shaft (diameter 8 mm and length 290 mm). One end of the stainless-steel shaft is connected with a flow velocity-sensing unit, which is composed of a rotor with five FEP blades (length 50 mm and width 20 mm) and 12 electrodes (length 50 mm and width 13 mm) circumferential uniformly distributed on the inner wall of the side cylinder. Different liquid level-sensing units for the liquid level comparison experiment: main and other electrodes with a width of 4 mm (Figure 4a); the width of the ordinary interdigital electrode 4 mm (Figure 4b); interdigital electrodes with widths of 4 and 12 mm in turn (Figure 4c) are investigated, respectively, uniformly distributed along the same PTFE tube (diameter 10 mm and thickness 1 mm). Finally, the acrylic cylinder is placed on the support frame to form the TNPFs.

Measurement of the TNPFs. First, the electrical signal of the TNPFs is transmitted to an electrometer (Keithley Model 6514). Second, the electrical output signal is collected and processed through a data acquisition system (NI-USB-6356, National Instruments) and LabVIEW software on a computer.

ASSOCIATED CONTENT

Supporting Information

The Supporting Information is available free of charge at <https://pubs.acs.org/doi/10.1021/acsami.1c20509>.

Principle analysis diagram of the connector of liquid level measurement for the TNPFs; instantaneous overflow area of the TNPFs when $h \leq R$; schematic diagram of stress analysis of the water wheel; COMSOL

simulation results of the potential distribution of water at different positions; output performance of the flow velocity-sensing unit in the TNPFs; the open-circuit voltage measured by the TNPFs liquid level-sensing unit at different liquid levels; the derivative curves of open-circuit voltage to time (dV_{OC}/dt) of three liquid level-monitoring methods under a liquid level of 100 mm; and performance of different width interdigital electrodes for the liquid level (PDF)

The demonstration of the TNPFs in the flow-monitoring system of a non-full pipe flow (Supporting Video S1) (MP4)

AUTHOR INFORMATION

Corresponding Authors

Tinghai Cheng – Beijing Institute of Nanoenergy and Nanosystems, Chinese Academy of Sciences, Beijing 101400, China; School of Mechatronic Engineering, Changchun University of Technology, Changchun, Jilin 130012, China; CUSTech Institute of Technology, Wenzhou, Zhejiang 325024, China; orcid.org/0000-0003-0335-7614; Email: chengtinghai@binn.cas.cn

Zhong Lin Wang – Beijing Institute of Nanoenergy and Nanosystems, Chinese Academy of Sciences, Beijing 101400, China; CUSTech Institute of Technology, Wenzhou, Zhejiang 325024, China; School of Materials Science and Engineering, Georgia Institute of Technology, Atlanta, Georgia 30332-0245, United States; orcid.org/0000-0002-5530-0380; Email: zhong.wang@mse.gatech.edu

Authors

Siyang He – Beijing Institute of Nanoenergy and Nanosystems, Chinese Academy of Sciences, Beijing 101400, China; School of Mechatronic Engineering, Changchun University of Technology, Changchun, Jilin 130012, China

Zheng Wang – Beijing Institute of Nanoenergy and Nanosystems, Chinese Academy of Sciences, Beijing 101400, China

Xiaosong Zhang – Beijing Institute of Nanoenergy and Nanosystems, Chinese Academy of Sciences, Beijing 101400, China; School of Mechatronic Engineering, Changchun University of Technology, Changchun, Jilin 130012, China

Zitang Yuan – Beijing Institute of Nanoenergy and Nanosystems, Chinese Academy of Sciences, Beijing 101400, China; School of Mechatronic Engineering, Changchun University of Technology, Changchun, Jilin 130012, China

Yushan Sun – School of Mechatronic Engineering, Changchun University of Technology, Changchun, Jilin 130012, China

Complete contact information is available at: <https://pubs.acs.org/doi/10.1021/acsami.1c20509>

Author Contributions

[†]S.H., Z.W., and X.Z. contributed equally to this work.

Notes

The authors declare no competing financial interest.

ACKNOWLEDGMENTS

The authors are grateful for the supports received from the Natural Science Foundation of Beijing Municipality (No. 3222023) and the National Key R&D Project from the Minister of Science and Technology (No. 2021YFA1201604).

REFERENCES

- (1) Wang, J.; Liu, G.; Wang, J.; Xu, X.; Shao, Y.; Zhang, Q.; Liu, Y.; Qi, L.; Wang, H. Current Status, Existent Problems, and Coping Strategy of Urban Drainage Pipeline Network in China. *Environ. Sci. Pollut. Res.* **2021**, *28*, 43035–43049.
- (2) Sun, B.; Chen, S.; Liu, Q.; Lu, Y.; Zhang, C.; Fang, H. Review of Sewage Flow Measuring Instruments. *Ain Shams Eng. J.* **2021**, *12*, 2089–2098.
- (3) Abda, F.; Azbaid, A.; Ensminger, D.; Fischer, S.; Francois, P.; Schmitt, P.; Pallarès, A. Ultrasonic Device for Real-Time Sewage Velocity and Suspended Particles Concentration Measurements. *Water Sci. Technol.* **2009**, *60*, 117–125.
- (4) Smith, J. Flowmeter Review. *Sens. Rev.* **1995**, *15*, 11–14.
- (5) Moosa, M.; Hekmat, M. Numerical Investigation of Turbulence Characteristics and Upstream Disturbance of Flow through Standard and Multi-Hole Orifice Flowmeters. *Flow Meas. Instrum.* **2019**, *65*, 203–218.
- (6) Leng, X.; Chanson, H. Integral Turbulent Scales in Unsteady Rapidly Varied Open Channel Flows. *Exp. Therm. Fluid Sci.* **2017**, *81*, 382–395.
- (7) Justensen, J.; Barfuss, S.; Johnson, M.; Meacham, T. Effect of Meter Orientation Downstream of a Short Radius Elbow on Electromagnetic Flow Meters. *J. Irrig. Drain. Eng.* **2019**, *145*, No. 06018009.
- (8) Ge, L.; Deng, H.; Wang, Q.; Hu, Z.; Li, J. Study of the Influence of Temperature on the Measurement Accuracy of Transit-Time Ultrasonic Flowmeters. *Sens. Rev.* **2019**, *39*, 269–276.
- (9) Sun, B.; Chen, S.; Liu, Q.; Lu, Y.; Zhang, C.; Fang, H. Review of Sewage Flow Measuring Instruments. *Ain Shams Eng. J.* **2021**, *12*, 2089–2098.
- (10) Fan, F.; Tian, Z.; Wang, Z. L. Flexible Triboelectric Generator. *Nano Energy* **2012**, *1*, 328–334.
- (11) Wang, Z. L.; Wang, A. C. On the Origin of Contact-Electrification. *Mater. Today* **2019**, *30*, 34–51.
- (12) Niu, S.; Liu, Y.; Chen, X.; Wang, S.; Zhou, Y.; Lin, L.; Xie, Y.; Wang, Z. L. Theory of Freestanding Triboelectric-Layer-Based Nanogenerators. *Nano Energy* **2015**, *12*, 760–774.
- (13) Wang, Z. L. On Maxwell's Displacement Current for Energy and Sensors: The Origin of Nanogenerators. *Mater. Today* **2017**, *20*, 74–82.
- (14) Wang, Z. L. On the First Principle Theory of Nanogenerators from Maxwell's Equations. *Nano Energy* **2020**, *68*, No. 104272.
- (15) Wang, Z. L. Catch Wave Power in Floating Nets. *Nature* **2017**, *542*, 159–160.
- (16) Wang, Z. L. Nanogenerators, Self-Powered Systems, Blue Energy, Piezotronics and Piezo-Phototronics-A Recall on the Original Thoughts for Coining These Fields. *Nano Energy* **2018**, *54*, 477–483.
- (17) Zhao, J.; Zhen, G.; Liu, G.; Bu, T.; Liu, W.; Fu, X.; Zhang, P.; Zhang, C.; Wang, Z. L. Remarkable Merits of Triboelectric Nanogenerator than Electromagnetic Generator for Harvesting Small-Amplitude Mechanical Energy. *Nano Energy* **2019**, *61*, 111–118.
- (18) Hu, W.; Zhang, C.; Wang, Z. L. Recent Progress in Piezotronics and Tribotronics. *Nanotechnology* **2019**, *30*, No. 042001.
- (19) Zhang, C.; Tang, W.; Han, C.; Fan, F.; Wang, Z. L. Theoretical Comparison, Equivalent Transformation, and Conjunction Operations of Electromagnetic Induction Generator and Triboelectric Nanogenerator for Harvesting Mechanical Energy. *Adv. Mater.* **2014**, *26*, 3580–3591.
- (20) Ahmed, A.; Saadatnia, Z.; Hassan, I.; Zi, Y.; Xi, Y.; He, X.; Zu, J.; Wang, Z. L. Self-Powered Wireless Sensor Node Enabled by a Duck-Shaped Triboelectric Nanogenerator for Harvesting Water Wave Energy. *Adv. Energy Mater.* **2017**, *7*, No. 1601705.
- (21) Wu, Z.; Cheng, T.; Wang, Z. L. Self-Powered Sensors and Systems Based on Nanogenerators. *Sensors* **2020**, *20*, 2925.
- (22) Wu, C.; Wang, A.; Ding, W.; Guo, H.; Wang, Z. L. Triboelectric Nanogenerator: A Foundation of the Energy for the New Era. *Adv. Energy Mater.* **2019**, *9*, No. 1802906.
- (23) Wang, Z. L. From Contact Electrification to Triboelectric Nanogenerators. *Rep. Prog. Phys.* **2021**, *84*, No. 096502.
- (24) Wang, Z. L. Triboelectric Nanogenerators as New Energy Technology and Self-Powered Sensors-Principles Problems and Perspectives. *Faraday Discuss.* **2014**, *176*, 447–458.
- (25) Jiang, D.; Xu, M.; Dong, M.; Guo, F.; Liu, X.; Chen, G.; Wang, Z. L. Water-Solid Triboelectric Nanogenerators: An Alternative Means for Harvesting Hydropower. *Renew. Sustain. Energy Rev.* **2019**, *115*, No. 109366.
- (26) Tang, W.; Chen, B.; Wang, Z. L. Recent Progress in Power Generation from Water/Liquid Droplet Interaction with Solid Surfaces. *Adv. Funct. Mater.* **2019**, *29*, No. 1901069.
- (27) Xie, Z.; Zeng, Z.; Wang, Y.; Yang, W.; Xu, Y.; Lu, X.; Cheng, T.; Zhao, H.; Wang, Z. L. Novel Sweep-Type Triboelectric Nanogenerator Utilizing Single Freewheel for Random Triggering Motion Energy Harvesting and Driver Habits Monitoring. *Nano Energy* **2020**, *68*, No. 104360.
- (28) Xu, Y.; Yang, W.; Yu, X.; Li, H.; Cheng, T.; Lu, X.; Wang, Z. L. Real-Time Monitoring System of Automobile Driver Status and Intelligent Fatigue Warning Based on Triboelectric Nanogenerator. *ACS Nano* **2021**, *15*, 7271–7278.
- (29) Heo, D.; Chung, J.; Kim, B.; Yong, H.; Shin, G.; Cho, J.; Kim, D.; Lee, S. Triboelectric Speed Bump as a Self-Powered Automobile Warning and Velocity. *Nano Energy* **2020**, *72*, No. 104719.
- (30) An, J.; Wang, Z.; Jiang, T.; Chen, P.; Liang, X.; Shao, J.; Nie, J.; Xu, M.; Wang, Z. L. Reliable Mechatronic Indicator for Self-Powered Liquid Sensing Toward Smart Manufacture and Safe Transportation. *Mater. Today* **2020**, *41*, 10–20.
- (31) Chen, B.; Tang, W.; He, C.; Deng, C.; Yang, L.; Zhu, L.; Chen, J.; Shao, J.; Liu, L.; Wang, Z. L. Water Wave Energy Harvesting and Self-Powered Liquid-Surface Fluctuation Sensing Based on Bionic-Jellyfish Triboelectric Nanogenerator. *Mater. Today* **2018**, *21*, 88–97.
- (32) Zhang, X.; Yu, M.; Ma, Z.; Ouyang, H.; Zou, Y.; Zhang, S.; Niu, H.; Pan, X.; Xu, M.; Li, Z.; Wang, Z. L. Self-Powered Distributed Water Level Sensors Based on Liquid-Solid Triboelectric Nanogenerators for Ship Draft Detecting. *Adv. Funct. Mater.* **2019**, *29*, No. 1900327.
- (33) Wang, Z.; Yu, Y.; Wang, Y.; Lu, X.; Cheng, T.; Bao, G.; Wang, Z. L. Magnetic Flap-Type Difunctional Sensor for Detecting Pneumatic Flow and Liquid Level Based on Triboelectric Nanogenerator. *ACS Nano* **2020**, *14*, 5981–5987.
- (34) Fu, X.; Bu, T.; Xi, F.; Cheng, T.; Zhang, C.; Wang, Z. L. Embedded Triboelectric Active Sensors for Real-Time Pneumatic Monitoring. *ACS Appl. Mater. Interfaces* **2017**, *9*, 32352–32358.
- (35) Wang, Z.; Gao, Q.; Wang, Y.; Wang, J.; Wang, Y.; Cheng, T.; Wang, Z. L. Triboelectric Flow Sensor with Float-Cone Structure for Industrial Pneumatic System Monitoring. *Adv. Mater. Technol.* **2019**, *4*, No. 1900704.
- (36) Wang, Y.; Wang, Z.; Zhao, D.; Yu, X.; Cheng, T.; Bao, G.; Wang, Z. L. Flow and Level Sensing by Waveform Coupled Liquid-Solid Contact-Electrification. *Mater. Today Phys.* **2021**, *18*, No. 100372.
- (37) Chen, J.; Tang, W.; Han, K.; Xu, L.; Chen, B.; Jiang, T.; Wang, Z. L. Bladeless-Turbine-Based Triboelectric Nanogenerator for Fluid Energy Harvesting and Self-Powered Fluid Gauge. *Adv. Mater. Technol.* **2019**, *4*, No. 1800560.
- (38) Jiang, P.; Zhang, L.; Guo, H.; Chen, C.; Wu, C.; Zhang, S.; Wang, Z. L. Signal Output of Triboelectric Nanogenerator at Oil-Water-Solid Multiphase Interfaces and Its Application for Dual-Signal Chemical Sensing. *Adv. Mater.* **2019**, *31*, No. 1902793.
- (39) Wen, Z.; Chen, J.; Yeh, M.; Guo, H.; Li, Z.; Fan, X.; Zhang, T.; Zhu, L.; Wang, Z. L. Blow-Driven Triboelectric Nanogenerator as an Active Alcohol Breath Analyzer. *Nano Energy* **2015**, *16*, 38–46.
- (40) Li, X.; Yeh, M.; Lin, Z.; Guo, H.; Yang, P.; Wang, J.; Wang, S.; Yu, R.; Zhang, T.; Wang, Z. L. Self-Powered Triboelectric Nanosensor for Microfluidics and Cavity-Confined Solution Chemistry. *ACS Nano* **2015**, *9*, 11056–11063.
- (41) Xu, M.; Wang, Y.; Zhang, S.; Ding, W.; Cheng, J.; He, X.; Zhang, P.; Wang, Z.; Pan, X.; Wang, Z. L. An Aeroelastic Flutter

Based Triboelectric Nanogenerator as a Self-Powered Active Wind Speed Sensor in Harsh Environment. *Extreme Mech. Lett.* **2017**, *15*, 122–129.

(42) Wang, J.; Ding, W.; Pan, L.; Wu, C.; Yu, H.; Yang, L.; Liao, R.; Wang, Z. L. Self-Powered Wind Sensor System for Detecting Wind Speed and Direction Based on a Triboelectric Nanogenerator. *ACS Nano* **2018**, *12*, 3954–3963.

(43) Xi, Y.; Guo, H.; Zi, Y.; Li, X.; Wang, J.; Deng, J.; Li, S.; Hu, C.; Cao, X.; Wang, Z. L. Multifunctional TENG for Blue Energy Scavenging and Self-Powered Wind-Speed Sensor. *Adv. Energy Mater.* **2017**, *7*, No. 1602397.

(44) Fu, X.; Xu, S.; Gao, Y.; Zhang, X.; Liu, G.; Zhou, H.; Lv, Y.; Zhang, C.; Wang, Z. L. Breeze-Wind-Energy-Powered Autonomous Wireless Anemometer Based on Rolling Contact-Electrification. *ACS Energy Lett.* **2021**, *6*, 2343–2350.

(45) Wang, P.; Zhang, S.; Zhang, L.; Wang, L.; Xue, H.; Wang, Z. L. An Ultra-Low-Friction Triboelectric Electromagnetic Hybrid Nanogenerator for Rotation Energy Harvesting and Self-Powered Wind Speed Sensor. *ACS Nano* **2018**, *12*, 9433–9440.

(46) Zhang, X.; Zheng, Y.; Wang, D.; Zhou, F. Solid-Liquid Triboelectrification in Smart U-Tube for Multifunctional Sensors. *Nano Energy* **2017**, *40*, 95–106.

(47) Cao, Y.; Shao, H.; Wang, H.; Yang, X.; Gao, Q.; Cheng, T.; Fang, J.; Lin, T. High-Linearity, Response-Range Adjustable Force Sensors Based on a Yarn/Film/Spacer Triboelectric Device Design. *Adv. Mater. Technol.* **2021**, *6*, No. 2100203.

(48) Shi, Q.; Wang, H.; Wang, T.; Lee, C. Self-Powered Liquid Triboelectric Microfluidic Sensor for Pressure Sensing and Finger Motion Monitoring Applications. *Nano Energy* **2016**, *30*, 450–459.

(49) Lin, S.; Chen, X.; Wang, Z. L. Contact Electrification at the Liquid-Solid Interface. *Chem. Rev.* **2021**, No. 1c00176.

(50) Wang, S. H.; Lin, L.; Wang, Z. L. Triboelectric Nanogenerators as Self-Powered Active Sensors. *Nano Energy* **2015**, *11*, 436–462.

(51) Zhang, C.; Liu, L.; Zhou, L.; Yin, X.; Wei, X.; Hu, Y.; Liu, Y.; Chen, S.; Wang, J.; Wang, Z. L. Self-Powered Sensor for Quantifying Ocean Surface Water Waves Based on Triboelectric Nanogenerator. *ACS Nano* **2020**, *14*, 7092–7100.

(52) Xu, M.; Wang, S.; Zhang, S.; Ding, W.; Kien, P. T.; Wang, C.; Li, Z.; Pan, X.; Wang, Z. L. A Highly-Sensitive Wave Sensor Based on Liquid-Solid Interfacing Triboelectric Nanogenerator for Smart Marine Equipment. *Nano Energy* **2019**, *57*, 574–580.

(53) Wang, W.; Wu, Y.; Chang, Z.; Chen, F.; Wang, H.; Gu, G.; Zheng, H.; Cheng, G.; Wang, Z. L. Self-Powered Intelligent Water Meter for Electrostatic Scale Preventing, Rust Protection, and Flow Sensor in a Solar Heater System. *ACS Appl. Mater. Interfaces* **2019**, *11*, 6396–6403.

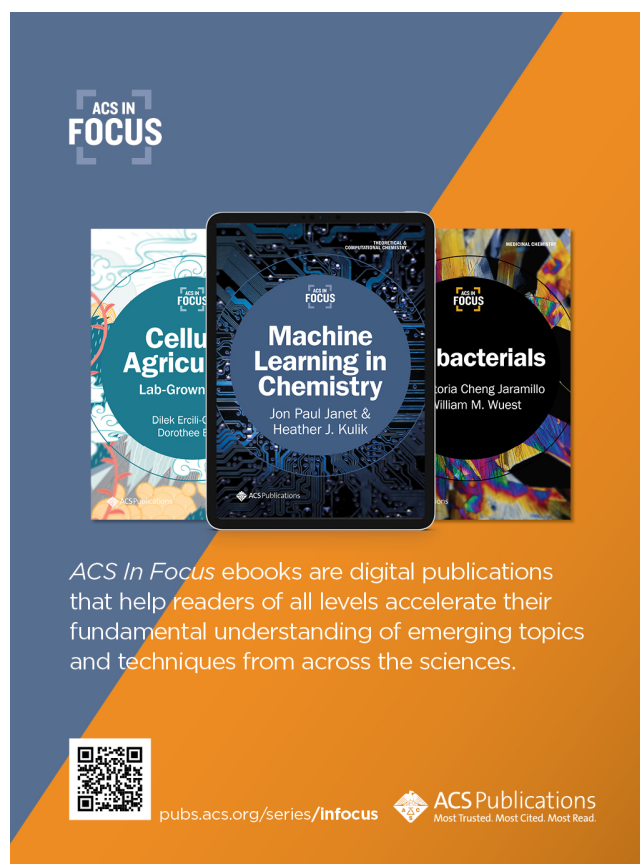
(54) Chen, J.; Guo, H.; Zheng, J.; Huang, Y.; Liu, G.; Hu, C.; Wang, Z. L. Self-Powered Triboelectric Micro Liquid/Gas Flow Sensor for Microfluidics. *ACS Nano* **2016**, *10*, 8104–8112.

(55) Xu, Y.; Yang, W.; Lu, X.; Yang, Y.; Li, J.; Wen, J.; Cheng, T.; Wang, Z. L. Triboelectric Nanogenerator for Ocean Wave Graded Energy Harvesting and Condition Monitoring. *ACS Nano* **2021**, *15*, 16368–16375.

(56) Xie, Z.; Dong, J.; Yang, F.; Xu, R.; Gao, Q.; Cheng, T.; Wang, Z. L. Sweep-Type Triboelectric Linear Motion Sensor with Staggered Electrode. *Extreme Mech. Lett.* **2020**, *37*, No. 100713.

(57) Wang, P.; Zhang, S.; Zhang, L.; Wang, L.; Xue, H.; Wang, Z. L. Non-Contact and Liquid-Liquid Interfacing Triboelectric Nanogenerator for Self-Powered Water/Liquid Level Sensing. *Nano Energy* **2020**, *72*, No. 104703.

(58) Wang, P.; Pan, L.; Wang, J.; Xu, M.; Dai, G.; Zou, H.; Dong, K.; Wang, Z. L. An Ultra-Low-Friction Triboelectric-Electromagnetic Hybrid Nanogenerator for Rotation Energy Harvesting and Self-Powered Wind Speed Sensor. *ACS Nano* **2018**, *12*, 9433–9440.



ACS IN FOCUS

Cellular Agriculture
Lab-Grown
Dilek Erilliç
Dorothee E.

Machine Learning in Chemistry
Jon Paul Janet & Heather J. Kulik

bacterials
Lidia Cheng Jaramillo
William M. Wuest

ACS In Focus ebooks are digital publications that help readers of all levels accelerate their fundamental understanding of emerging topics and techniques from across the sciences.

pubs.acs.org/series/infocus

ACS Publications
Most Trusted. Most Cited. Most Read.

QR code